# Thin Film Characterizations Using XRD

## The Cases of $VO_2$ and NbTiN

College of William & Mary

Conner Geery

November 26, 2014

# Contents

# 1 Introduction

Materials in thin film form often have different properties than in their bulk form, and in many cases it is possible to exploit such different properties in applications. The different properties arise primarily from the geometry of the film, since a large proportion of the atoms in the sample are exposed to different environment than in bulk, when they are either at the surface or the interface. The main topic of this thesis is to showcase the microstructure properties of two different materials in thin film form. Vanadium dioxide is a particularly interesting compound that exhibits an insulator to metal transition that can be induced by applying heat, light pulses, or electric fields. When $VO_2$ is in its insulating state at room temperature, it is transparent to infrared light; however, it becomes metallic above its transition temperature ($68^o$ C for bulk $VO_2$) and it reflects light. Applications for this behavior have many possibilities, smart windows, infrared filters, and optical switches being a few.

Our objective in growing our $VO_2$ thin films is to maximize the $VO_2$ content in our samples such that the changes in optical transmission are more dramatic. In doing this, we will be able to confirm our hypothesis that there is a correlation between our samples' microstructure and their transition from an insulator to a metal. Thus far, we have been able to moderately prove this correlation due to the change in our thin films' increase in transmission change after annealing.

NbTiN superconducting thin films coated inside superconducting radio frequency (SRF) cavities have been proposed as possible means to enhance cavity performance. It is important to examine the structure and surface morphology of these thin films in order to assess a correlation with their performance for such application. Used in particle accelerators, at present these SRF cavities are made of bulk niobium, a superconductor kept at or below 9.24 K in order to maintain its superconducting properties. However, technical constraints regarding intrinsic material properties limit its capabilities, thus indicating the need to explore NbTiN and its superconducting properties as a thin film. Our objective in examining NbTiN is to prove correlation between the thin film samples' physical properties and their ability to effectively superconduct.

X-ray diffraction is one particular method for studying the microstructure of these films. In the present case it was performed with a research class instrument, the PANalytical Empyrean, a machine capable of High-resolution X-ray diffraction (HRXRD). HRXRD is a technique that provides non-destructive analysis of crystalline structured materials. We were able to extract important information from the experimental data using programs such as Data Collector, HighScore, and Origin Pro.

I will further discuss the results of our x-ray diffraction and engage in further discussion of our testing of the properties of $VO_2$ and its heat-induced insulator to metal transition. This transition was measured using a custom-built setup including an infrared HeNe laser and a thermocouple connected with our samples, providing a method for testing change in

transmission of our samples. Through changing growth parameters during film deposition, we have been able to enhance useful properties of our $VO_2$ and NbTiN thin film samples but further work is needed to enhance their properties.

# 2 Experimental Techniques

Below is a description of the experimental techniques used and their fundamental principles.

## 2.1 X-Ray Diffraction

X-ray diffraction (XRD) is used to study microstructure due to the nanometer scale of the crystalline lattice parameters and the fact that x-rays have wavelengths on the order of Angstroms.

A four-circles diffractometer is needed to characterize the microstructure of thin films to ensure proper alignment between the diffraction plane and the plane of the actual thin film sample. In this case we have used the Empyrean instrument by PANalytical. The Empyrean machine was used for measurements at $2\theta$, $2\theta - \omega$, $\omega$, and z in order to align and evaluate our samples. The incident angle, $\omega$, is defined between the X-ray source and the sample. The diffracted angle, $2\theta$, is defined between the incident beam and the detector angle, where the incident beam and detector are both at adjustable angles to the sample stage. A scan adjusting both $2\theta$ and $\omega$ simultaneously is performed for each diffraction peak in order to study phase and compound composition of our samples, while a scan adjusting only $\omega$ (rocking curve) is run to study defects and optimize a subsequent $2\theta - \omega$ scan (Speakman). Each of these scans is interpreted using Data Collector paired with the machine, and HighScore to closely examine the location of peaks, The compounds present can be deduced from the observed diffraction peaks and the and Miller indices they typically represent.

### 2.1.1 Bragg's Law & Scherrer Equation

Particular crystalline structures produce XRD peaks at predictable angles. We use Bragg's law to identify a specific peak in order to characterize the structure of our samples, determining lattice parameters, i.e. the spacing between crystal planes, with the equation

$$n\lambda = 2dsin\theta, \tag{2.1}$$

where $n$ is an integer, $\lambda$ is the wavelength of the incident X-ray, $d$ is the spacing between planes in the crystal lattice, and $\theta$ is the incident angle of the X-ray and the plane of the thin film. Given the relation

$$d = \frac{a}{\sqrt{h^2 + k^2 + l^2}}, \tag{2.2}$$

with $a$ representing lattice spacing in the crystal and $h$, $k$, and $l$ being the Miller indices of the plane, we can combine equations 2.1 and 2.2 to determine lattice spacing in the crystal with the following equation:

$$(\frac{\lambda}{2a})^2 = \frac{sin^2\theta}{h^2 + k^2 + l^2}. \tag{2.3}$$

Using this equation and Miller indices that match the peaks that we see in the reflected X-rays for a certain plane, we can determine the microstructure of our samples. Different geometries affect the observable peaks corresponding to different Miller indices in a crystal. For example, for crystals that are body-centered cubic (bcc), we can see peaks at Miller indices whose sum is even. We can compare the locations of peaks we expect to see with data to asses the actual microstructure of the samples.

In our XRD analysis, we also measured the full width of the peaks at half the maximum intensity (FWHM) in order to determine the grain size in the films, using the Scherrer equation. This is written as

$$\tau = \frac{K\lambda}{\beta cos\theta}, \tag{2.4}$$

with $\tau$ as the mean grain size, $K$ as a shape factor (typically close to 0.9), and $\beta$ as the FWHM. It is important to note that the Scherrer equation is applicable to particles smaller than about $0.1-0.2\mu$ m. Using our XRD scans, we used Origin Pro to determine the location and FWHM of our peaks.

## 2.2 Metal Insulator Transition

A unique property of $VO_2$ is that it transitions from an insulator to a metal with the use of heat, among other things. The transition that $VO_2$ encounters is first order, and accompanied by a structural phase transition. In its transition from high to low temperatures, $VO_2$ transitions from a rutile tetragonal structure to a monoclinic distortion of this structure in which vanadium ions create pairs. These pairs are then off-axis from the original structure of the vanadium, resulting in a displacement of the vanadium atom. The metal-insulator transition (MIT) in $VO_2$ is thus a result of this antiferroelectric displacement (Zylbersztejn and Mott [1975]). For the present work, the transition was measured for each sample using an HeNe infrared laser and detector while heating and cooling the film.

# 3 Experiments

I started my XRD practice with NbTiN, in order to familiarize myself with the XRD technique. After gaining sufficient experience, I began to concentrate my efforts on $VO_2$ and will be focusing on $VO_2$ for this project.

## 3.1 Testing with NbTiN

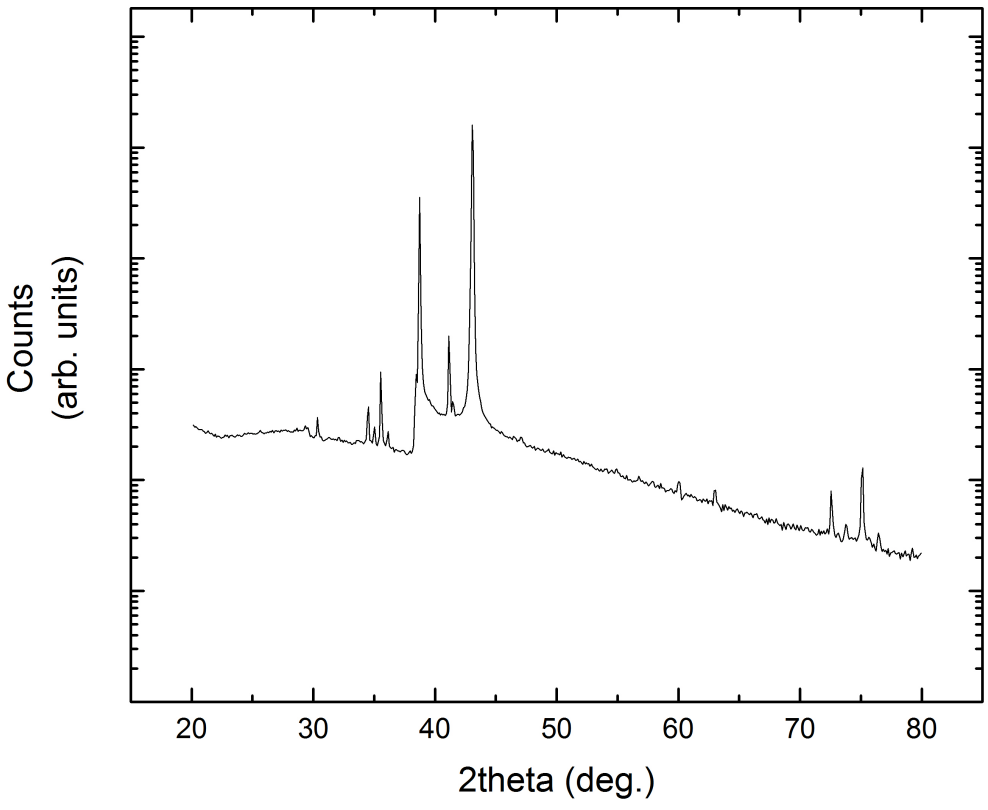


Figure 3.1: **Example of NbTiN XRD peaks.**

NbTiN thin films' microstructure affects their superconducting properties. In Fig. 3.1, a typical XRD scan of a NbTiN sample, used for further analysis by other collaborators, is shown.

At present, the growth of such films is being investigated. We are using XRD to examine how changes in various parameters will affect and improve their growth and subsequent superconducting properties.

## 3.2 $VO_2$

Studying $VO_2$ more in depth, I have experience with XRD and the optical investigation of the insulator to metal transition that our samples exhibit upon increasing their temperature from room temperature up to about $71^o$ C. We have found that the growth parameters when depositing our films clearly affect the XRD, which in turn also affects the change in optical transmission of infrared light in our samples. This indicates a clear correlation between the composition of the samples as revealed by the microstructure analysis and its transitional properties.

### 3.2.1 XRD

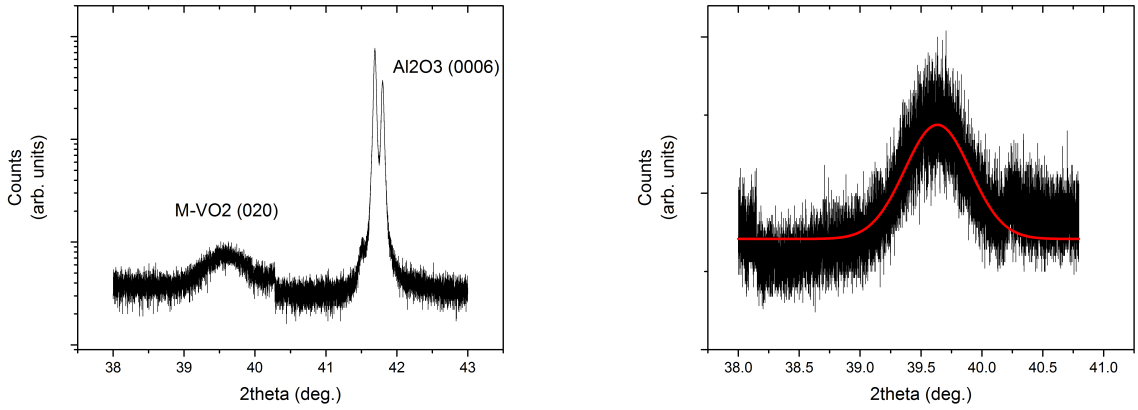


Figure 3.2: **Example of $VO_2$ sample XRD peaks.** XRD peaks in sample 031314, with a closer image of the $VO_2$ peak.

Using XRD, other oxide phases typically encountered were $V_2O_5$ and $V_5O_9$ in our samples. Notably, the samples that produced the largest change in transmission of infrared light had lower concentrations of these oxide phases in relation to pure $VO_2$, and thus it was easier to optimize on the $VO_2$ peaks for these samples rather than optimizing on the substrate peaks; optimization on the substrate peak can be seen in Fig. 3.2.

### 3.2.2 MIT

We probed the change in transmission under infrared light as our samples were heated and cooled. A detector behind the stage provided a voltage reading related to the amount of the infrared light transmitted through the sample. We heat our samples from $26.32^o$ C

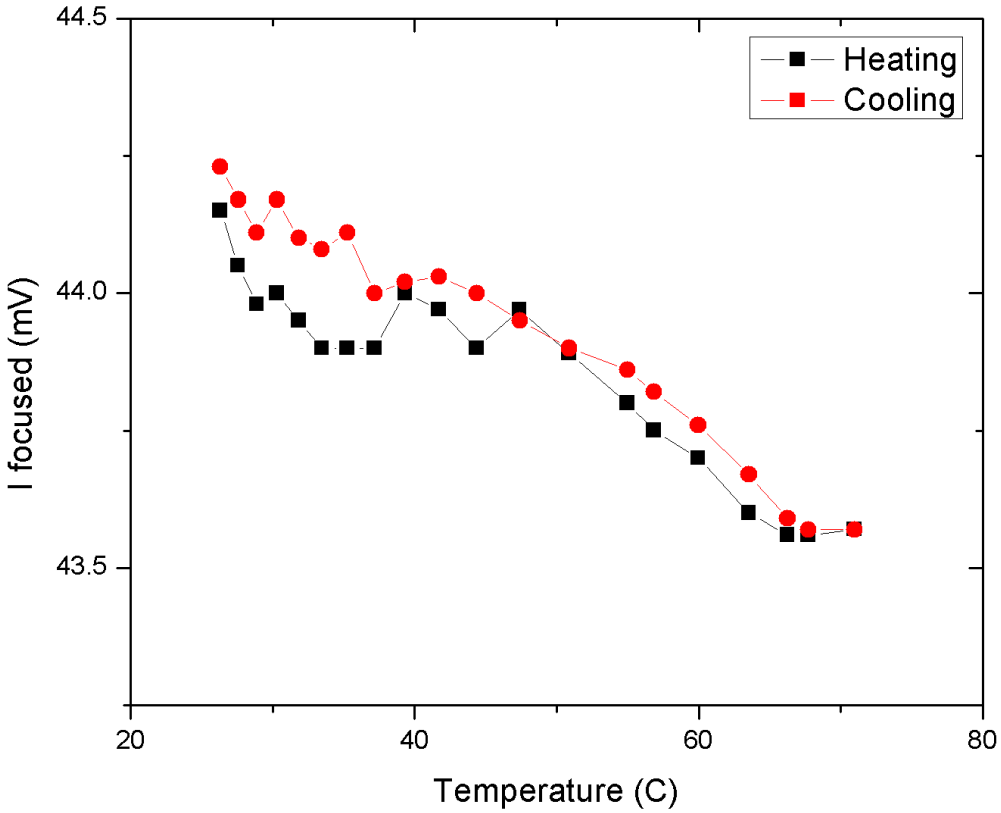


Figure 3.3: **Example of Hysteresis of $VO_2$ Transmission Change.** Transmission change in sample 031314.

to 70.97$^o$ C, and the insulator to metal transition (MIT) temperature was around 68$^o$ C. This thermally induced transition leads to increased conductivity in the samples with a corresponding decrease in infrared transmission indicating its metallic state (Wang et al. [2014]). The change in transmission measured in our samples can be plotted as a function of temperature (Fig. 3.3).

### Samples

We are continuing to examine samples 052114, 052214, 060214, 060914, and 061014, as their drop in transmission is remarkably greater than others. Each of these samples' XRD peaks display only $VO_2$ and substrate. We hope to improve their transitions by re-annealing the samples in nitrogen, and we will continue by completing further XRD and MIT measurements afterwards.

### 3.2.3 Growth

Aside from growing reproducible samples, our main mission is to find optimal growing conditions for a greater change in infrared transmission. In growing our thin films, we use a DC magnetron sputtering process; this is the simplest and most reproducible method, making it optimal for what we are trying to achieve. During magnetron sputtering, we sputter vanadium targets to achieve thickness for our films (20 mins = 20 nm) with 4.5mTorr of argon gas, keeping the substrate at $600^o$ C. The films are then oxidized by thermal annealing at the same temperature with $O_2$ levels varying between 0.31-1 mTorr for times varying from 30 mins to 4 hrs. We have most recently been re-annealing our samples after oxidation. The heat introduced to our samples results in a release of oxygen, leading over-oxidized phases to become pure $VO_2$.

# 4 Results

We have been able to achieve a moderate rate of reproducibility for our $VO_2$ thin films, which warrants more efforts. Re-annealing our samples after oxidation may improve transmission changes since over-oxidized compounds ($V_2O_5$) that we typically see in $VO_2$ samples are lessened with this treatment. Our most successful samples are shown in Table 4.1. Since none of these samples had any oxide phases aside from pure $VO_2$, we can infer that the structural properties of our thin film samples have a direct effect on their ability to transition from an insulator to a metal. The transition seen in $VO_2$ is a consequence of a structural change, leading the structural properties of our samples to be an important factor in the change in transmission.

Some problems with our growing process were found due to due to lack of a valve to better control mass-flow ratio during thin film processing in our growing system. With the recent installation of that valve, our growing parameters will be easier to control and offer more predictable effects, since such valve enables the control of the flow mass onto the substrate, which is critical to achieve specific compounds.

| Sample Name | Sample | V Thickness | $O_2$ Temp. | $O_2$ Pressure | $O_2$ Time | Post-$O_2$ Anneal Temp. | Post-$O_2$ Anneal Time | XRD Peaks | MIT (Trans.) |
|---|---|---|---|---|---|---|---|---|---|
| 031314 | $VO_x$/c-$Al_2O_3$ | 45nm | 500° C | 1 mTorr | 1 hr | | | $VO_2$(020) $V_2O_5$(820) | .03978% .31032% |
| 052114 | $VO_x$/c-$Al_2O_3$ | 45nm | 500° C | 1 mTorr | 1 hr | | | $VO_2$(020) * | .76235% .79107% |
| 032014 | $VO_x$/c-$Al_2O_3$ | 45nm | 500° C | 1 mTorr | 30 min | | | $VO_2$(020) $V_2O_5$(820), $V_5O_9$ | .34382% .30100% |
| 052214 | $VO_x$/c-$Al_2O_3$ | 45nm | 500° C | 1 mTorr | 30 min | | | $VO_2$(020) * | .76235% .75097% |
| 032714 | $VO_x$/c-$Al_2O_3$ | 30nm | 500° C | 1 mTorr | 20 min | | | $VO_2$(020) $V_2O_5$(820), $V_5O_9$ | .30829% .31002% |
| 052314 | $VO_x$/c-$Al_2O_3$ | 30nm | 500° C | 1 mTorr | 20 min | | | $VO_2$(020) $V_2O_5$(820), $V_5O_9$ | .37810% .38451% |
| 040214 | $VO_x$/c-$Al_2O_3$ | 30nm | 500° C | 1 mTorr | 10 min | | | $VO_2$(020) $V_2O_5$(820), $V_5O_9$ | .28717% .28138% |
| 041514 | $VO_x$/c-$Al_2O_3$ | 30nm | 300° C | 1 mTorr | 30 min | | | $VO_2$(020) $V_2O_5$(820), $V_5O_9$ | .38926% .38958% |
| 042514 | $VO_x$/c-$Al_2O_3$ | 30nm | 300° C | 1 mTorr | 20 min | | | $VO_2$(020) $V_2O_5$(820), $V_5O_9$, $V_6O_{13}$ | .57134% .56597% |
| 051214 | $VO_x$/c-$Al_2O_3$ | 30nm | 300° C | 1 mTorr | 10 min | | | $VO_2$(020) $V_2O_5$(820), $V_5O_9$ | .24418% .24526% |
| 060214 | $VO_x$/c-$Al_2O_3$ | 45nm | 500° C | 1 mTorr | 30 min | 600° C | 30 min (vacuum) | $VO_2$(020) * | 1.095% 1.078% |
| 060914 | $VO_x$/c-$Al_2O_3$ | 20nm | 500° C | 1 mTorr | 1 hr | | | $VO_2$(020) * | .98725% 1.0055% |
| 061014 | $VO_x$/c-$Al_2O_3$ | 20nm | 500° C | 1 mTorr | 30 min | | | $VO_2$(020) * | .71595% .71199% |
| 021714 | $VO_x$/c-$Al_2O_3$ | 45nm | 500° C | 1 mTorr | 2 hr | | | $VO_2$(020) $V_2O_5$(820), $V_2O_3$(306) | .16919% |
| 022714 | $VO_x$/c-$Al_2O_3$ | 45nm | 600° C | 0.51 mTorr | 4 hr | | | Surface crack | -- |
| 022814 | $VO_x$/c-$Al_2O_3$ | 45nm | 500° C | 0.31 mTorr | 2 hr | | | $V_2O_5$(820) | -- |
| 030614 | $VO_x$/c-$Al_2O_3$ | 45nm | 500° C | 0.51 mTorr | 2 hr | | | $V_2O_5$(820) | -- |
| 032114 | $VO_x$/c-$Al_2O_3$ | 45nm | 500° C | 0.8 mTorr | 1 hr | | | $VO_2$(020) $V_2O_5$(820), $V_5O_9$ | .43754% .44034% |

Figure 4.1: **$VO_2$ Transmission Change.** Evidence of increased drop in transmission with re-annealing. *XRD performed with new optics

# 5 Summary and Outlook

We have successfully shown a correlation between the structural properties of our $VO_2$ thin film samples and their ability to transition from an insulator to a metal. We must further our efforts towards repeatable samples and more consistent growth parameters, and continue our XRD and MIT measurements following changes in our growing procedure.

In the future, we plan on further examining our samples with XRD correlate it with our MIT response after re-annealing them in nitrogen. We also plan on using a 4 point probe to test the resistivity changes across the MIT, thus determining the exact temperature of transition in our samples.

In studies done elsewhere, it has been reported that lattice strain or element doping in $VO_2$ are useful in altering its transition temperature. A lower transition temperature is useful in practical applications of $VO_2$ for smart window material. One of the most commonly used elements used for this purpose is tungsten, proven to lower transition temperatures very close to room temperature (Peng et al.). Samples with lower transition temperatures exhibit changes in resistance and abrupt transition behaviors unseen in normal transition temperatures, however (Li and Dho [2014]).

Using photo-induced transitions during XRD measurement has also proven useful for examining the change in material (Hada et al. [2010]). Extensive research on $VO_2$ has also been done with $TiO_2$ substrates rather than sapphire (c-$Al_2O_3$). Roughness values for these samples are slightly larger than those with sapphire substrates. Also recorded was an interdiffusion of the $VO_2$ and $TiO_2$ that was not noted in previous samples with sapphire substrates (Li and Dho [2014]).

# Bibliography

Masaki Hada, Kunio Okimura, and Jiro Matsuo. Characterization of structural dynamics of vo2 thin film on c-al2o3 using in-air time-resolved x-ray diffraction. Physical Review B, 82(15), October 2010.

Jian Li and Joonghoe Dho. Characteristics of phase transition of vo2 films grown on tio2 substrates with different crystal orientations. Journal of Crystal Growth, 404:84–88, October 2014.

Scott S. Speakman. Introduction to hrxrd. Massachusetts Institute of Technology.

L. Wang, I. Novikova, J. M. Klopf, S. Madaras, G. P. Williams, E. Madaras, and R. A. Lukaszew. Distinct length scales in the vo2 metal-insulator transition revealed by bichromatic optical probing. Advanced Optical Materials, pages 30–33, 2014.

A. Zylbersztejn and N. F. Mott. Metal-insulator transition in vanadium dioxide. Physical Review B, 11(11):4383–4395, 06 1975.